Human Molecular Genetics, 2018, Vol. 27, No. 11 1913–1926

doi: 10.1093/hmg/ddy098
Advance Access Publication Date: 16 March 2018
Original Article

ORIGINAL ARTICLE

Mutations in the mitochondrial ribosomal protein *MRPS22* lead to primary ovarian insufficiency

Anlu Chen[1,‡], Dov Tiosano[2,3,‡], Tulay Guran[4,‡], Hagit N. Baris[3,5,‡], Yavuz Bayram[6,†,‡], Adi Mory[5], Laura Shapiro-Kulnane[7], Craig A. Hodges[7,8], Zeynep C. Akdemir[6], Serap Turan[4], Shalini N. Jhangiani[9], Focco van den Akker[1], Charles L. Hoppel[10], Helen K. Salz[7], James R. Lupski[6,9,11,12] and David A. Buchner[1,7,13,*]

[1]Department of Biochemistry, Case Western Reserve University, Cleveland, OH 44106, USA, [2]Division of Pediatric Endocrinology, Ruth Children's Hospital, Rambam Medical Center, Haifa 30196, Israel, [3]Rappaport Family Faculty of Medicine, Technion—Israel Institute of Technology, Haifa 30196, Israel, [4]Department of Pediatric Endocrinology and Diabetes, Marmara University Hospital, Istanbul 34899, Turkey, [5]The Genetics Institute, Rambam Health Care Campus, Haifa 3109601, Israel, [6]Department of Molecular and Human Genetics, Baylor College of Medicine, Houston, TX 77030, USA, [7]Department of Genetics and Genome Sciences and [8]Department of Pediatrics, Case Western Reserve University, Cleveland, OH 44106, USA, [9]Human Genome Sequencing Center, Baylor College of Medicine, Houston, TX 77030, USA, [10]Department of Pharmacology, Center for Mitochondrial Diseases, Case Western Reserve University, Cleveland, OH 44106, USA, [11]Department of Pediatrics, Baylor College of Medicine, Houston, TX 77030, USA, [12]Texas Children's Hospital, Houston, TX 77030, USA and [13]Research Institute for Children's Health, Case Western Reserve University, Cleveland, OH 44106, USA

*To whom correspondence should be addressed at: Department of Genetics, School of Medicine, Case Western Reserve University, 2109 Adelbert Road, Cleveland, OH 44106-4935, USA. Tel: +1 2163681816; Fax: +1 2163681835; Email: dab22@case.edu

Abstract

Primary ovarian insufficiency (POI) is characterized by amenorrhea and loss or dysfunction of ovarian follicles prior to the age of 40. POI has been associated with autosomal recessive mutations in genes involving hormonal signaling and folliculogenesis, however, the genetic etiology of POI most often remains unknown. Here we report *MRPS22* homozygous missense variants c.404G>A (p.R135Q) and c.605G>A (p.R202H) identified in four females from two independent consanguineous families as a novel genetic cause of POI in adolescents. Both missense mutations identified in *MRPS22* are rare, occurred in highly evolutionarily conserved residues, and are predicted to be deleterious to protein function. In contrast to prior reports of mutations in *MRPS22* associated with severe mitochondrial disease, the POI phenotype is far less severe. Consistent with this genotype—phenotype correlation, mitochondrial defects in oxidative phosphorylation or rRNA levels were not detected in fibroblasts derived from the POI patients, suggesting a non-bioenergetic or tissue-specific mitochondrial

[†]Present address: Department of Genetics and Genomic Sciences, Icahn School of Medicine at Mount Sinai, New York, NY 10029, USA.
[‡]These authors contributed equally to this work.
Received: February 20, 2018. **Revised:** March 13, 2018. **Accepted:** March 14, 2018

defect. Furthermore, we demonstrate in a Drosophila model that mRpS22 deficiency specifically in somatic cells of the ovary had no effect on fertility, whereas flies with mRpS22 deficiency specifically in germ cells were infertile and agametic, demonstrating a cell autonomous requirement for mRpS22 in germ cell development. These findings collectively identify that MRPS22, a component of the small mitochondrial ribosome subunit, is critical for ovarian development and may therefore provide insight into the pathophysiology and treatment of ovarian dysfunction.

Introduction

Primary ovarian insufficiency (POI) is defined by the loss or dysfunction of ovarian follicles associated with amenorrhea before the age of 40 (1). POI is a major cause of female infertility with a prevalence greater than 1%. There is a strong genetic component to the development of POI, both in the form of monogenic and multigenic disorders, however, in most cases the genetic etiology of POI remains unclear (2). Among the most common genetic defects associated with POI are X chromosome defects, which collectively account for approximately 10–25% of POI cases (2). These include Turner's syndrome, Triple X syndrome and Fragile X syndrome. A number of monogenic disorders resulting in POI have also been identified, including those with variants in *BMP15* and *PGRMC1*, both located on Chromosome X, as well as those with variants in *GDF9*, *FOXO3*, *FIGLA* and *NR5A1*, among others, that are autosomal (2). These variants are each estimated to account for between 1% and 2% of POI cases. Thus, the majority of POI cases remain classified as idiopathic.

Although there remains much to understand about the genetic basis of POI, much has been learned already about both normal and pathological ovarian development based on cellular and molecular studies of the genes that have been associated with POI. For example, SYCE1, STAG3 and HFM1 are members of the synaptonemal complex that are required for chromosomal segregation during meiosis (3–7) and NUP107 is a component of the nuclear pore complex that is important for maintaining the communication between gonadal somatic cells and oocytes (8). Furthermore, autosomal recessive disorders that affect DNA repair, such as *MCM8* (9) and *MCM9* (10,11) and genes encoding transcription factors, such as *FIGLA* (12), *SOHLH1* (13) and *NOBOX* (14,15) have been recently reported in POI. Moreover, eukaryotic translation initiation factor 4E nuclear import factor 1 (*eIF4ENIF1*) has been recently identified in cases of dominantly inherited POI (16). However, there are still many cases with unexplained POI suggesting that new causative genes are yet to be discovered.

Here we present the identification of two different homozygous missense mutations in the nuclear-encoded gene mitochondrial ribosomal protein S22, *MRPS22*, as another genetic cause of POI in four adolescent females from two independent consanguineous families. Drosophila modeling demonstrated a cell autonomous function of the *MRPS22* ortholog in germ cells that is required for female germ cell viability, thus collectively demonstrating the importance of MRPS22 in reproduction and ovarian development.

Results

Identification of mutations in *MRPS22* in patients with POI

To identify novel genetic causes of POI, we focused on an extended Israeli-Christian Arab consanguineous family, in which two distinct genetic conditions with autosomal-recessive inheritance patterns were suspected (Fig. 1A). The presence of two distinct genetic conditions is not uncommon in this particular patient population (17). The first genetic condition presented as 46, XY females with inguinal hernias that contained testicles in two twin sisters at the age of 3 years (Fig. 1A, F1-IV-7 and F1-IV-8). Genetic evaluation revealed that both sisters had a 46, XY karyotype and were homozygous for a missense mutation in the hydroxysteroid 17-beta dehydrogenase 3 gene [NM_000197.1 (*HSD17B3*): c.239G>A; p.Arg80Gln], thus resulting in a diagnosis of 17-beta hydroxysteroid dehydrogenase type III deficiency (OMIM: 605573) (18). *HSD17B3* converts androstenedione to testosterone and is expressed predominantly in the testes (19). One girl underwent bilateral gonadectomy at the age of 3 years and continued to be raised as a female. Her sister underwent unilateral gonadectomy at the age of 3 years and was raised as female until the age of 9 years, when due to adrenarche and the presence of one testicle in the inguinal canal, signs of masculation appeared. The parents decided to raise the child as a boy. All of the other girls in the extended family (Fig. 1A) were evaluated and found to have a normal 46, XX karyotype.

The second genetic condition in this family was suspected when the proband (Fig. 1A, F1-IV-9) presented with delayed puberty at the age of 16 years, with delay in breast development (B) and pubic hair (P) that were at Tanner stage 1 and 2, respectively. Hormonal testing revealed hypergonadotrophic hypogonadism as evidenced by high basal gonadotropin levels including luteinizing hormone (LH) and follicle-stimulating hormone (FSH), as well as undetectable estradiol (E2) (Table 1). Medical history revealed normal pregnancy and delivery (birth weight 3000 g) and normal growth and development during childhood. Genetic analysis revealed that this individual was homozygous for the p.Arg80Gln variant in the *HSD17B3* gene. However, all previously described 46, XX female patients that were homozygous for the p.Arg80Gln variant were asymptomatic (18,20). Thus, a second unrelated genetic condition was suspected (17). Family history revealed that in the extended family there is another 19-year-old girl (Fig. 1A, F1-IV-5) with delayed puberty (B1P2) and a similar profile of POI with hypergonadotrophic hypogonadism (Table 1). MRI of the proband demonstrated a very small uterus, measuring $5 \times 12 \times 14$ mm. Adrenocorticotropic hormone (ACTH) testing in both patients confirmed normal cortisol production, without any evidence of an enzymatic block (Supplementary Material, Table S1). Urinary steroid analysis by gas chromatography/mass spectrometry (GC/MS) revealed low levels of etiocholanolone (Et) and androsterone (An), and that methemoglobin levels were normal. Echocardiography revealed a normal heart in both sisters. Lactate levels (1.0 and 1.4 mmol/L; normal range 0.5–1.6 mmol/L) and blood pH (pH = 7.33 and 7.31) were both normal. Bone age measurements taken at chronological age 18 years and 3 months were compatible with bone age of 13 years, thus demonstrating delayed bone age.

The proband's sister (Fig. 1A, F1-IV-11), at the age of 9 years also showed elevated LH level of 10.4 mIU/ml with low FSH 0.27 mIU/ml and undetectable estrogens. At the age of 12 years,

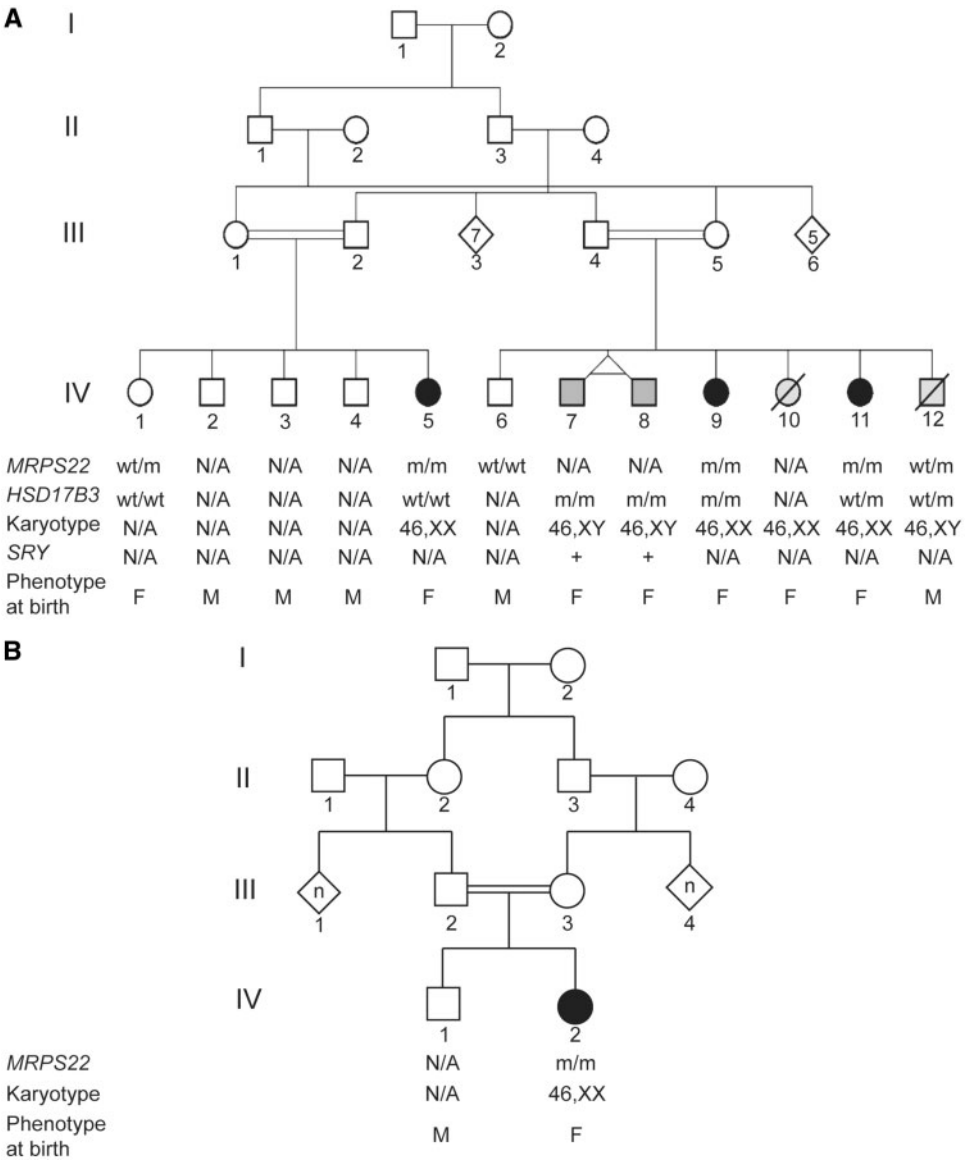

Figure 1. Pedigrees of two consanguineous families with POI. (**A**) Family I pedigree structure. Below the pedigree are the genotypes corresponding to *MRPS22*, *HSD17B3* and the karyotyping results. *MRPS22* mutation refers to c.605G>A; p.Arg202His. *HSD17B3* mutation refers to c.239G>A; p.Arg80Gln. (**B**) Family II pedigree structure. Below the pedigree are the *MRPS22* genotypes, which refers to c.404G>A; p.Arg135Gln and the karyotyping results.

Table 1. Hormone levels in four individuals with POI

	F1-IV-5	F1-IV-9	F1-IV-11	F2-IV-2	Normal pubertal range
Age (years)	19	16	12	14	
LH (mIU/l)	17.3	21.0	9.1	20.0	1.0–14.7
FSH (mIU/l)	41.3	78.0	21.0	99.4	3.0–21.0
E2 (pmol/l)	Not detected	Not detected	141	0.04	55–1250

physical examination revealed Tanner stage 3 breast development with detectable estrogen but elevated gonadotropins (Table 1). Anti-mullerian hormone was undetectable < 0.16 µg/l. MRI showed a small uterus with normal cervix ($21 \times 9 \times 9$ mm) and small ovaries ($10 \times 6 \times 4$ mm). An ovarian biopsy at the age of 14 years, taken for ovarian tissue preservation, demonstrated fibrotic ovaries without follicles (Fig. 2). All three affected individuals are the offspring of first degree cousins, consistent with an autosomal recessive inheritance pattern (Fig. 1A). Genetic evaluation in all three patients revealed a normal female karyotype 46, XX. One patient was homozygous for the p.Arg80Gln variant in *HSD17B3*, one was heterozygous and one did not carry the *HSD17B3* variant. Given that mutations in *HSD17B3* are not associated with POI (18,20), and the POI phenotype did not segregate with the p.Arg80Gln variant in *HSD17B3* in this family, it suggested an independent genetic etiology (Fig. 1A).

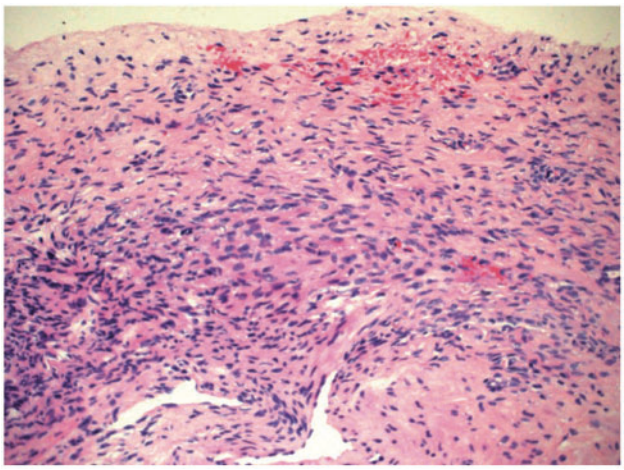

Figure 2. Absence of germ cells in the ovary of a female patient with the *MRPS22* p.R202H mutation. H & E-stained ovarian tissue from individual F1-IV-9.

To identify the genetic basis of the POI, linkage analysis was performed with affected individuals F1-IV-5, F1-IV-9 and the unaffected sibling F1-IV-1. Based on the predicted autosomal recessive inheritance pattern, we focused on regions of homozygosity in the affected daughters F1-IV-5 and F1-IV-9 that were heterozygous in the unaffected sibling F1-IV-1. SNP genotyping analysis identified 19 loci greater than 1 Mb on 10 different chromosomes that segregated with the POI.

To identify the causal genetic mutation within these candidate intervals, we performed WES in affected individual F1-IV-5 and the unaffected individual F1-IV-1 (Fig. 1A). Candidate variants encoding non-synonymous changes discovered by WES were filtered to remove variants with an allele frequency greater than 0.01 and that were not predicted by either SIFT (21) or Polyphen2 (22) to be damaging or possibly damaging to protein function. After filtering, four candidate variants from Family I were left and were validated by Sanger sequencing. However, only the variant in mitochondrial ribosomal protein S22 [*MRPS22*, NM_020191.2: c.605G>A: p.R202H; ClinVar Variation ID SCV000607729], segregated with the POI phenotype in Family I with 30 unaffected and three affected family members. Based on the SNP linkage analysis, this variant was within a 3 Mb interval defined by the SNP markers rs2737735 and rs16850488 on Chromosome 3 that segregated with POI. Analysis of polymorphisms within the WES data revealed an absence of heterozygosity within this interval (Fig. 3A). To ensure that there were no other non-synonymous variants within this interval segregating with disease, the 12 coding regions of genes that were not covered by WES were analyzed by Sanger sequencing. These 12 intervals totaled 2167 bp of coding sequence (average size: 197 bp; range 53–411 bp) (Supplementary Material, Table S2). No additional variants were identified, demonstrating that the *MRPS22* (p.R202H) variant was the only amino acid change that segregated with disease. This variant is present in dbSNP (rs753345594) but has an allele frequency of 0.00001218 (3/246 212), with no homozygotes present in the genome Aggregation Database (gnomAD, v2.0). The Arg202 residue is highly evolutionarily conserved (Fig. 3B). Collectively, this data suggested that the *MRPS22* (p.R202H) variant was a strong candidate as a novel genetic cause of POI.

To identify additional POI patients with a mutation in *MRPS22*, this gene was submitted to GeneMatcher (23). A second family was identified in which WES revealed a different homozygous missense mutation in *MRPS22* [NM_020191; c.404G>A; p.R135Q; ClinVar Variation ID SCV000693853] in the proband F2-IV-2. This variant was confirmed by Sanger sequencing and was located within a genomic interval defined by an absence of heterozygosity (Fig. 3A). Exome variant analysis had led to initial prioritization of five homozygous candidate variants in Family II, in *BCL6*, *KDM1A*, *MRPS22*, *PLXND1* and *TRIM62*. This patient presented with a POI phenotype similar to that described for the three patients in Family 1 and as described in detail below. The *MRPS22* variant was not present in the Greater Middle East Variome Project WES database (24), the Genome Aggregation Database (gnomAD) (25) or the BCM-HGSC internal database that consists of more than 6500 exomes including ~1100 Turkish exomes. Moreover, similar to *MRPS22* (p.R202H), this variant is highly evolutionarily conserved (Fig. 3B) and predicted to be deleterious to protein function by SIFT and Polyphen2 (21,22).

In Family II, the proband (F2-IV-2) was born to first degree cousins of Turkish descent (Fig. 1B). She presented with amenorrhea at 14 years and 8 months of age. Her previous medical history revealed normal pregnancy and delivery at term but she was small for gestational age with 1900 grams birth weight (−3.9 SDS). Family history was not consistent with a sexual development, puberty or infertility disorder. Physical examination revealed mild facial dysmorphism including deep-set eyes with mild hypotelorism and mild ptosis, thin upper lip and hypoplastic nares. Height was 145.3 cm (−2.1 SDS) and weight was 45 kg (+0.4 SDS). At chronological age of 14 years and 8 months, bone age was 10 years. Fundoscopy was normal. She had Tanner stage 3 breast development, without pubic or axillary hair development. Laboratory evaluation revealed a normal 46, XX female karyotype and normal blood count and chemistry except for impaired glucose tolerance test. Blood pH levels were normal (pH = 7.42), however, blood lactate concentrations were slightly elevated (3 mmol/L; normal range 0.5–1.6 mmol/L) and nerve conduction studies and electromyography testing revealed bilateral axonal polyneuropathy at lower extremities as indicated by absent evoked potentials from bilateral sural, peroneal and tibial nerves. Brain and heart morphology was normal, as revealed by cranial and pituitary MRIs and echocardiography, respectively. Endocrine evaluation revealed hypergonadotrophic hypogonadism (Table 1). Abdomino-pelvic ultrasound showed small uterus of 15 × 12 × 3 mm, and ovaries could not be visualized. ACTH test was normal (Supplementary Material, Table S1). Plasma adrenal steroids by LC-MS/MS confirmed very low keto steroids (Table 2). Methemoglobin levels were elevated (1.9%, normal range: 0–1.5%) and DXA revealed mild osteoporosis (L2–L4, Z-score −2.1, BMD: 0.736 g/cm^2). She was treated with combined estrogen and progesterone supplementation and had menarche at 16 years and 8 months. Her final height is 157 cm (+0.4 SDS) and weight is 58 kg (+1 SDS). Pelvic ultrasound at 20 years of age showed uterus as 42 x 21 x 8 mm and hypoplastic ovaries (right ovary: 14 × 6 × 4 mm; left ovary: 11 × 8 × 4 mm).

Cellular studies of POI patient-derived fibroblasts

Collectively, the identification of two independent families with POI and predicted deleterious missense mutations in *MRPS22* was highly suggestive that pathogenic variants in this gene represent a novel genetic cause of POI. To examine the role of the *MRPS22* (p.R202H) variant on gene function, MRPS22 mRNA and protein expression levels were examined in patient-derived fibroblasts. No detectable changes were identified in protein or

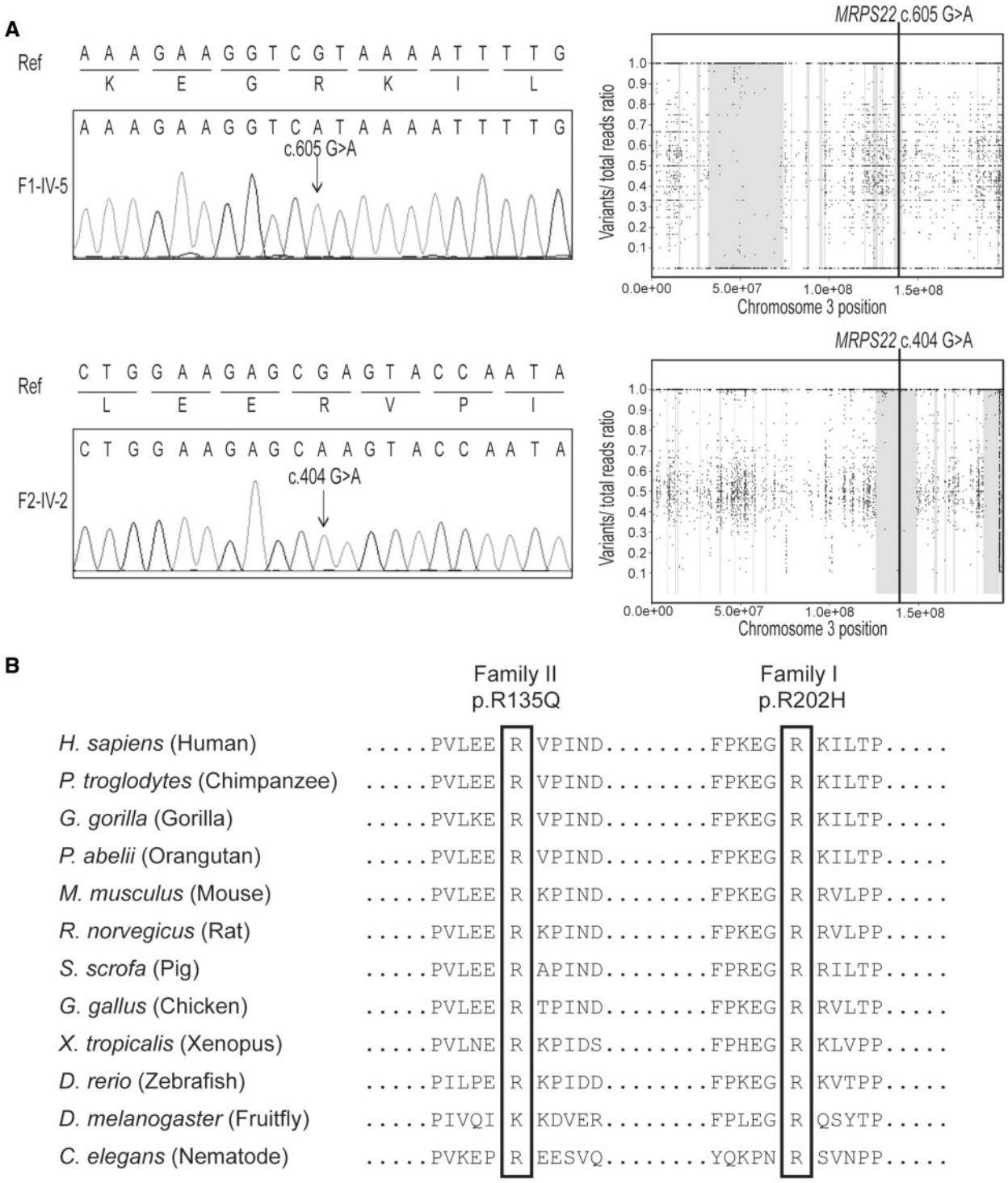

Figure 3. Independent mutations in *MRPS22* identified in two consanguineous families with POI. **(A)** Sanger sequencing confirms the presence of the *MRPS22* mutations detected by WES. Intervals with an absence of heterozygosity were identified based on calculated B-allele frequencies from the WES data. Gray-shaded areas indicate regions with an absence of heterozygosity. The location of *MRPS22* within an interval with an absence of heterozygosity is indicated by a vertical black line. **(B)** Alignment of protein sequences of MRPS22 from multiple species demonstrates the evolutionary conservation of the MRPS22 residues Arg135 and Arg202 that are altered in patients with POI.

mRNA expression levels between control- and patient-derived primary fibroblasts (Fig. 4A and B). In addition to potential expression level differences in MRPS22, as a component of the small subunit of the mitochondrial ribosome, defects in MRPS22 have been shown to reduce the levels of mitochondrial rRNAs (26,27). However, there were no differences between control- and patient-derived fibroblasts in the expression levels of the 12S and 16S rRNA expression levels (Fig. 4C).

To evaluate the effect of *MRPS22* (p.R202H) on mitochondrial function, we performed mitochondrial function studies in

control- and patient-derived primary fibroblasts. Measurements of electron transport chain complex enzyme activities from cultured skin fibroblasts and OXPHOS activity measured with permeabilized cells both failed to identify significant differences in activity between fibroblasts from the POI patients and control individuals (Fig. 5). Thus, *MRPS22* (p.R202H) has no detectable effect on mitochondrial function in primary fibroblasts, although we were unable to directly examine its function in ovarian tissue.

Table 2. Plasma adrenal steroid levels in two individuals with POI

	F1-IV-9	F2-IV-2	Normal range
Progesterone (nmol/l)	0.9	0.54	0.5–2.3
DHEAS (μmol/l)	0.7	0.9	1.8–10.3
DHEA (nmol/l)	Not done	1.1	3.5–41.1
Androstendione (nmol/l)	3.3	0.02	1.7–16.3
Testosterone (nmol/l)	<0.3	0.3	0.3–3.8

Embryonic lethality of Mrps22 deficient mice

Given the inability to study the impact of the *MRPS22* mutations in patient-derived ovarian tissue, we generated two animal models to better investigate the *in vivo* function of MRPS22. First, we examined a homozygous *Mrps22* knockout mouse model that was generated by complete deletion of all exons and intervening sequences. Heterozygous *Mrps22* knockout mice (+/–) were fertile and showed no overt signs of abnormalities. However, among 3-week-old offspring of a heterozygous intercross, no homozygous knockout mice (–/–) were detected (Table 3). Similarly, when offspring of a heterozygous intercross were genotyped at embryonic day 18.5 (e18.5), again no –/– offspring were

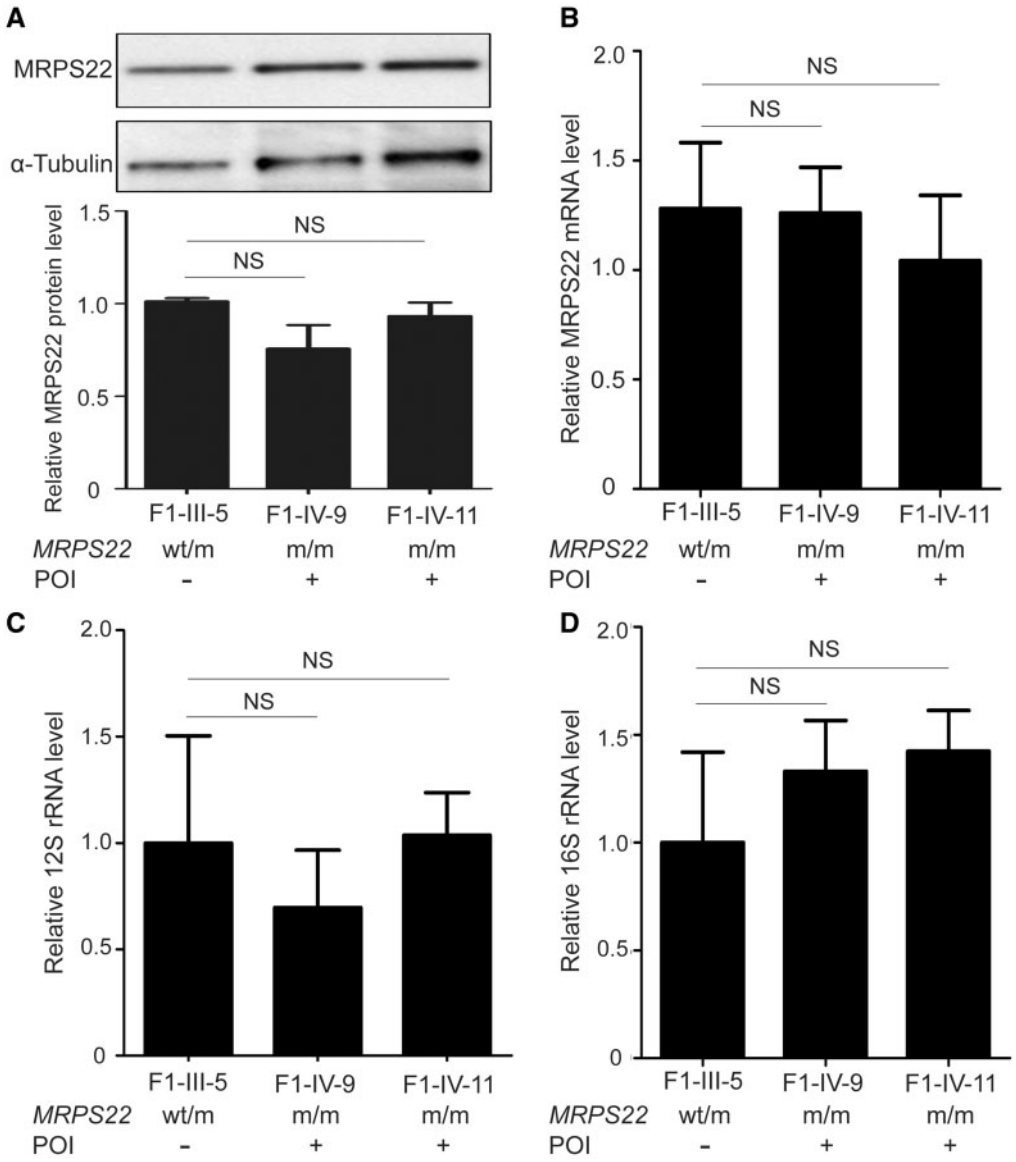

Figure 4. Molecular analysis of fibroblasts from patients with the *MRPS22* (p.R202H) mutation. (**A**) Western blot analysis of MRPS22 and the loading control alpha-tubulin from control- and patient-derived primary fibroblasts. Levels of MRPS22 protein were determined by ImageJ analysis and normalized to alpha-tubulin. (**B**) Levels of *MRPS22* mRNA, (**C**) 12S rRNA, and (**D**) 16S rRNA were detected by RT-qPCR and were unchanged between control- and patient-derived fibroblasts. NS, not significant.

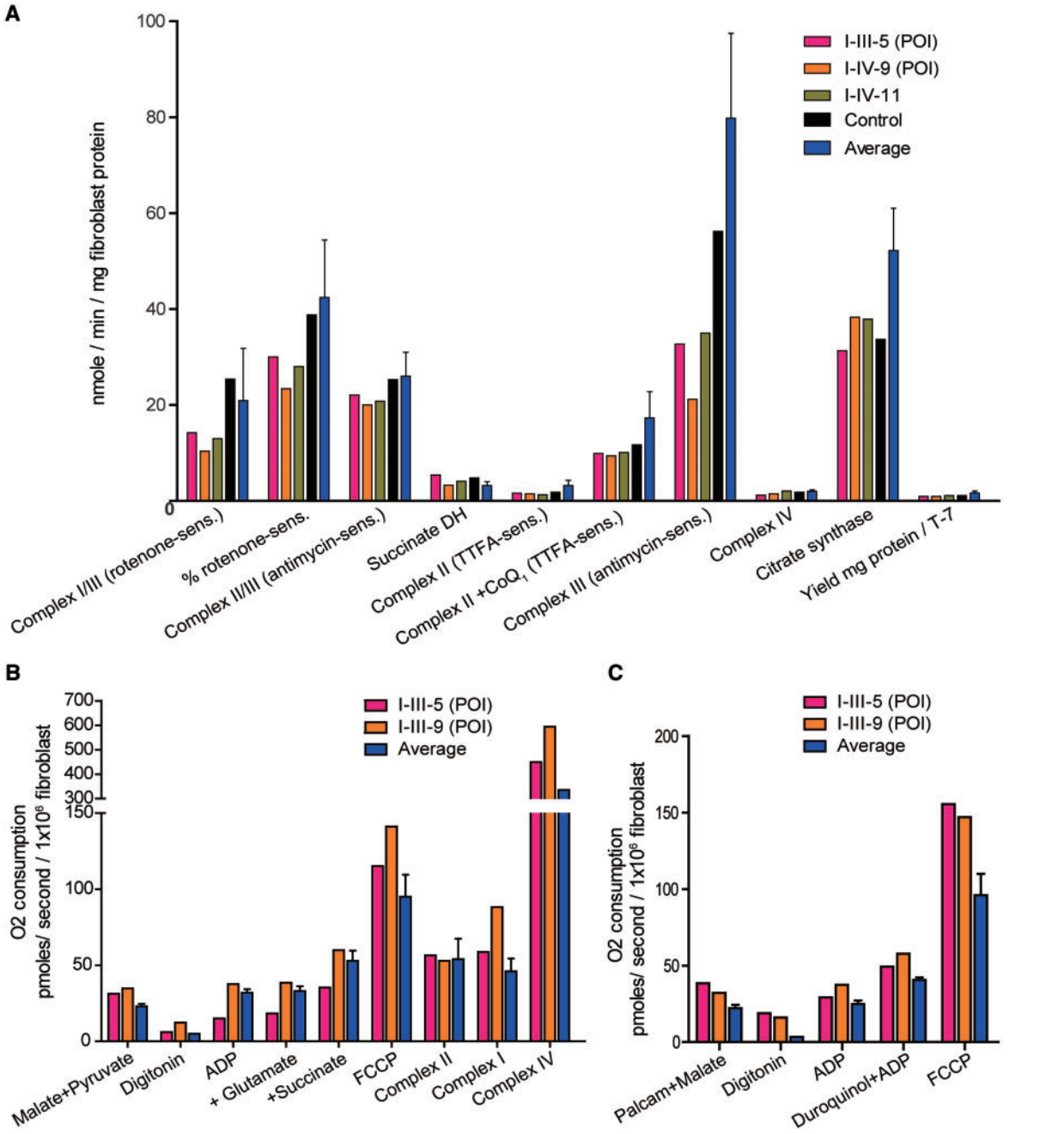

Figure 5. Oxidative phosphorylation is normal in fibroblasts from patients with the *MRPS22* (p.R202H) mutation. (**A**) Intact mitochondria isolated from fibroblasts were supplied with electron donor substrates and respiration, as indicated by oxygen uptake, was measured with a Clark electrode. (**B**) Rate of oxidative phosphorylation in fibroblasts determined using protocol 1 as described (53). (**C**) Rate of oxidative phosphorylation in fibroblasts determined using protocol 2 as described (53). Control samples denote a genetically unrelated fibroblast line of approximately equal passage number that was analyzed concurrently with the samples derived from Family I. Average denotes the historical averages of control samples analyzed from a reference population (electron transport chain activity, $n = 144$; oxidative phosphorylation, $n = 57$). Average sample is shown as mean ± standard deviation. None of the data in the POI individuals is significantly different from the controls.

detected (Table 3). Thus, complete deficiency of Mrps22 results in embryonic lethality, demonstrating the crucial role of Mrps22 in development, but preventing functional studies in adult ovarian tissue.

mRpS22 in *Drosophila* germ cells is required for fertility

The *Drosophila melanogaster* genome encodes a single ortholog, *mRpS22*, with significant homology to the human *MRPS22* gene. To evaluate the role of mRpS22 *in vivo*, we used an inducible tissue-specific RNA interference (RNAi)-mediated knockdown approach. In these experiments, knockdown was achieved by expressing a short hairpin RNA under the control of the upstream activator sequence (UAS) with the following drivers: *tub-Gal4* which uniformly drives expression in all tissues (28); *c587-Gal4*, and *bab-Gal4*, which drive expression in the somatic cells of the ovary (29); and the germline-specific *nos-Gal4:: VP16* driver (30). We found that ubiquitous *mRpS22* knockdown

(*tub > mRpS22*^{RNAi}) resulted in larval death. Interestingly, we found that knockdown in germ cells (*nos > mRpS22*^{RNAi}), but not in the somatic cells of the ovary, led to female sterility (Table 4).

To identify the defect underlying the female sterility, ovaries were stained with an antibody against Vasa, which labels all germ cells, and the DNA stain DAPI to monitor germ cell differentiation. Adult ovaries are composed of 15–20 individual strands of progressively developing egg chambers called ovarioles (Fig. 6A). Egg chambers are assembled within the germarium, a structure at the anterior end of each ovariole. Each egg chamber contains 16 interconnected germ cells, one of which will become an oocyte and the others polyploidy nuclei. As each 16-cell cyst is surrounded by an epithelial monolayer of somatic cells, it will bud off from the germarium to form a chain of individualized egg chambers of progressive age. The *bab > mRpS22*^{RNAi} mutant ovarioles were indistinguishable from those in wild-type flies, suggesting that loss of mRpS22 in the somatic cells of the ovary did not alter cell viability or ovarian development (Fig. 6B). However, *nos > mRpS22*^{RNAi} mutant ovarioles lacked strings of developing egg chambers (Fig. 6C). Moreover, no germ cells were detected, even at the tip of the ovariole where the germline stem cells normally reside. (Fig. 6C) This agametic phenotype suggests a defect in germ cell survival.

Discussion

Here we describe the identification of four individuals from two independent consanguineous families with missense mutations in *MRPS22* that result in autosomal recessive inheritance of POI. The conclusion of pathogenicity for the *MRPS22* variants was based on the cumulative evidence stemming from the identification of two different homozygous missense variants in independent families together with functional data from a Drosophila model of germ cell-specific *mRpS22* deficiency. The genetic data supports the causal role of the *MRPS22* variants based on the following ACMG criteria: absence in population databases (strength of criteria = pathogenic moderate), multiple lines of computational evidence supporting a deleterious effect on the gene (pathogenic supporting) and co-segregation with disease in multiple affected family members (pathogenic moderate). In addition, despite the absence of mitochondrial defects in functional studies of patient-derived fibroblasts (benign strong), the animal modeling studies in Drosophila demonstrated a deleterious effect of *mRpS22* deficiency on fertility and ovarian development (pathogenic strong). Thus, the cumulative evidence together supports the pathogenicity of homozygous *MRPS22* missense variants as a novel cause of POI in adolescents.

MRPS22 encodes a component of the small 28S mitochondrial ribosome subunit that is found in species including mammals, fruit flies and nematodes but lacks a direct ortholog in fungi, yeast, plants or bacteria (31). Protein translation in mitochondria is required to translate the 13 polypeptides encoded in the mitochondrial genome that are essential components of all mitochondrial respiratory chain complexes, excluding complex II which is entirely nuclear encoded (32). The mitochondrial ribosome is composed of 80 proteins and three rRNA molecules divided between two subunits, a large 39S subunit and a small 28S subunit (33,34). Beyond *MRPS22*, mutations in other nuclear-encoded proteins involved in mitochondrial translation are associated with impaired ovarian development. Homozygous mutations in another component of the 28S subunit, *MRPS7*, were associated with primary hypogonadism and primary adrenal failure as well as sensorineural deafness and lactic academia (35). Mutations in the mitochondrial tRNA synthetases *HARS2* and *LARS2* both result in Perrault syndrome consisting of sensorineural hearing loss and ovarian dysfunction (36,37). Mutations in the mitochondrial tRNA synthetase *AARS2* cause progressive leukoencephalopathy with ovarian failure (38). Finally, mutations in any of the five subunits of *EIF2B* can lead to ovarioleukodystrophy, which in addition to vanishing white matter in the nervous system is associated with ovarian failure in female carriers (39). Thus, the causal relationship between mutations in many genes involved in mitochondrial translation and ovarian development highlight the critical role of mitochondrial translation in this tissue.

In addition to mutations in *MRPS22* causing POI, rare mutations in *MRPS22* have also previously been reported to cause severe mitochondrial disease with features including cardiomyopathy, lactic acidosis and brain abnormalities (26,27,40,41). Features related to ovarian or germ cell development were not previously reported in these patients. Therefore, this report extends the phenotypic spectrum of disorders associated with impaired MRPS22 function. The only previous case reports of female patients with *MRPS22* mutations were three female infants who were homozygous for an *MRPS22* (p.R170H) allele and presented with severe hypotonia, hypertrophic cardiomyopathy, lactic acidosis and died in infancy. Patients described in three other case reports were all males, and also presented in critical condition with heart and brain abnormalities. Molecular analysis of mitochondrial function in patient-derived fibroblasts from these patients identified decreased enzyme activities for the oxidative phosphorylation complexes and decreased levels of mitochondrial 12S and 16S rRNAs. Thus, the pathogenic variants p.R170S and p.L215P in *MRPS22* in these patients compromised mitochondrial energy production. This is in contrast to the POI patient fibroblasts carrying the *MRPS22* c.605G>A: p.R202H mutation, which demonstrated no defects in OXPHOS activity or mitochondrial rRNA levels. This is consistent with the relatively milder phenotype of POI and the absence of lactic acidosis. Collectively, this suggests that the *MRPS22* mutations p.R202H and p.R135Q associated with POI affect primarily the mitochondrial role in the reproductive system but not in global energy production.

Table 3. Survival of offspring from a *Mrps22* heterozygous knockout mouse (+/−) intercross

Age	E18.5			3 weeks		
Genotype	+/+	+/−	−/−	+/+	+/−	−/−
Observed	12	25	0	10	22	0
Expected	9.25	18.5	9.25	8	16	8
P-value		0.0021			0.0046	

Table 4. Phenotypes of RNAi-mediated mRpS22 tissue-specific knockdown in *Drosophila*

RNAi driver	Conditional knockdown	Survival condition	Female fertility
tub-Gal4	Whole body	Larval lethality	—
bab-Gal4	Ovary: somatic cells	Viable	Fertile
c587-Gal4	Ovary: somatic cells	Viable	Fertile
nos-Gal4	Ovary: germ cells	Viable	Infertile

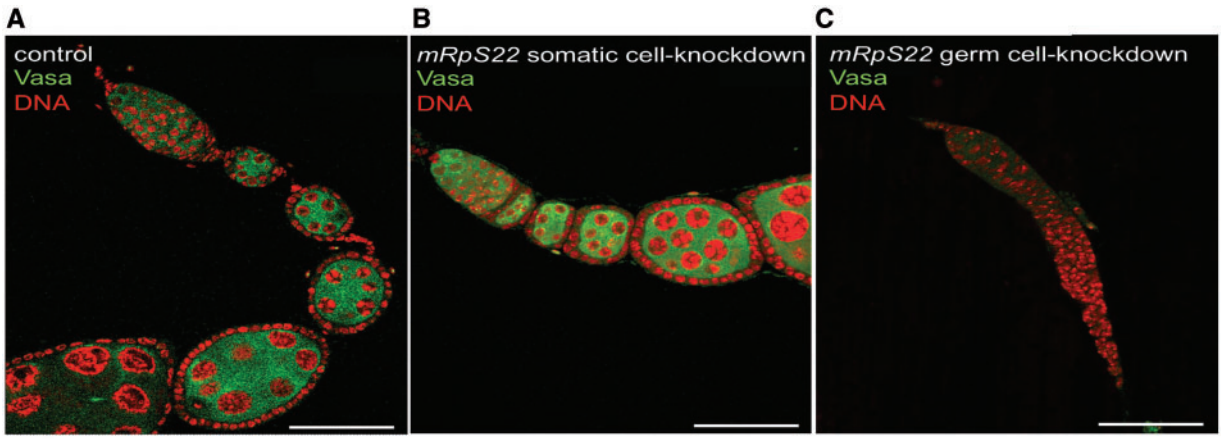

Figure 6. mRpS22 is required for female germ cell development in *Drosophila*. Representative confocal images of ovarioles from (**A**) control, (**B**) $bub > mRpS22^{RNAi}$ and (**C**) $nos > mRpS22^{RNAi}$ females stained for the cytoplasmic Vasa protein (green) to visualize germ cells, and the DNA stain DAPI (red). Scale bar: 50 μm.

Structural analysis of the human mitochondrial ribosome (33) suggests a potential mechanism for the more severe phenotypes associated with the missense mutations p.L215P (27) and p.R170H (26) relative to the relatively milder POI phenotype associated with the p.R135Q and p.R202H mutations (Fig. 7). Amino acids R135 and R202 are buried and situated in an internal region of MRPS22, between an α-helical subdomain and a β-sheet + 1 α-helix subdomain as shown above and below the cluster containing R202 and R135 (Fig. 7). Both R135 and R202 form hydrogen bond interactions and van der Waals interactions that will be disrupted by their respective mutations causing a localized disturbance of that particular MRPS22 structure, possibly also affecting its interaction with residues near F177 of MRPS18B. The L215 residue is located in a hydrophobic region comprised of three α-helices. The p.L215P mutation likely not only causes a disruption of this hydrophobic core, but the change to Pro is also predicted to disrupt both the hydrogen bonding of the α-helix to which L215 belongs and van der Waals interactions with an α-helix of MRPS18B (Fig. 7). The R170 residue is situated in the β-sheet + 1 α-helix subdomain (Fig. 7). The R170 side chain is making a hydrogen bond interaction with the backbone oxygen of S162. This S162 residue itself is in hydrogen bonding distance with D71 of protein MRPS16 (Fig. 7). We anticipate that the p.R170H mutation will cause loss of the interaction with S162 of MRPS22 and thereby lead to an altered conformation of this region. In summary, the anticipated structural consequences of the R135Q and R202H are likely similar as they are in close proximity to each other (~8.5Å) and are part of the same buried charge cluster in between two subdomains of MRPS22 (Fig. 7). In contrast, the R170H and L215P mutations are postulated to indirectly cause disruption of protein: protein interfaces (Fig. 7).

The etiology of ovarian dysfunction due to mutations in *MRPS22*, and other proteins that function in mitochondrial translation, remains unclear (42). However, the fact that germ-cell specific deletion of *mRpS22* in Drosophila results in agametic ovaries suggests a cell autonomous phenotype within the female germline. Interestingly, the precursors to these cells, primordial germ cells, demonstrate significantly elevated OXPHOS activity relative to other cell types (43). Furthermore, this activity is important for the eventual specification of these stem cells (43). The critical dependence of primordial germ cells on high levels of OXPHOS may contribute to the specific ovarian dysgenesis phenotype in the context of relatively mild impairments in mitochondrial translation, as other cell types are unaffected by the subtle mitochondrial defects. Thus, the identification of mutations in specific genes that cause these mild mitochondrial defects and are therefore critical for oocyte formation will lead to a better understanding of normal ovarian development and potentially a better understanding of the molecular basis of premature ovarian failure.

Materials and Methods

Human studies

These studies were approved by the ethics committees of Rambam Health Care Campus, Marmara University, and the Baylor-Hopkins Center for Mendelian Genomics. Informed consent was obtained from all participants. Peripheral blood was collected from affected individuals, parents and unaffected relatives if available. Genomic DNA was extracted from blood leukocytes according to standard procedures.

Linkage analysis

Individuals F1-IV-5, F1-IV-9 and F1-IV-1, were genotyped at loci across the genome using the Illumina Omni 250K SNP chip. Based on the presumed autosomal recessive model of inheritance, regions of homozygosity greater than 1 megabase were identified that were shared between the affected individuals F1-IV-5 and F1-IV-9, but not the control individual F1-IV-1.

Whole exome sequencing

Whole exome sequencing (WES) of patient F1-IV-5 and control individual F1-IV-1 was performed at The Technion Institute Sequencing Core. DNA was extracted from whole blood and sequencing using the Illumina TruSeq kit. Samples were sequenced with paired-end 100 bp reads totaling 19 290 546 for sample F1-IV-5 and 18 997 336 for sample F1-IV-1. The fastq sequence files were mapped to the reference human genome GRCh37 using BWA (v. 0.7.5) (44). Sequence was analyzed following the GATK (v. 2.8-1) best practices including removal of duplicate reads by Picard (v. 1.105), local realignment and base quality score recalibration (45). The resulting number of unique mapped reads for F1-IV-5 and F1-IV-1 were 17 785 392 and 14 074 730, respectively. The average read depth was 15.3× and

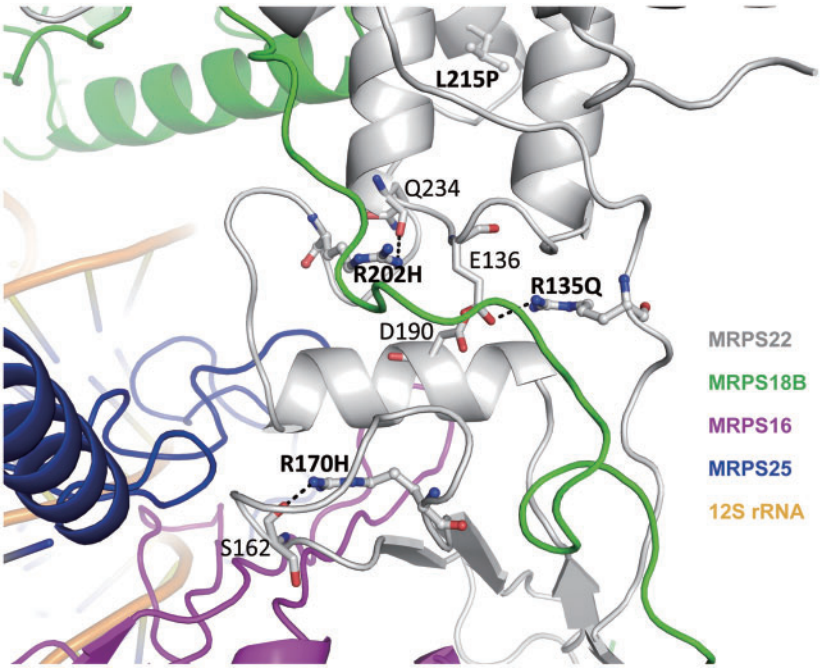

Figure 7. Structural analysis of disease-causing missense mutations in *MRPS22*. Close-up view of the human mitochondrial ribosome structure containing the four identified disease-causing missense mutations in *MRPS22*. The mitochondrial ribosome structure (39) (PDBid = 3j9m) is shown in cartoon representation with the mutations shown in ball-and-stick and nearby key residue in stick representation. The ribosomal proteins MRPS22, MRPS18B, MRPS16 and MRPS25 and the 12S rRNA are colored grey, green, magenta, blue and orange, respectively. Hydrogen bonds are depicted by dashed lines. The figure was generated using PYMOL (htttps://pymol.org).

14.7× respectively. HaplotypeCaller was used to call SNPs and indels (45). For SNPs, the filters used were QD < 2.0, FS > 60.0, and MQ < 40.0. For indels, the filters used were QD < 2.0 and FS > 200.0. The variants passing these filters were annotated with Annovar (46) using the following databases: nonsyn_splicing, esp6500si_all, 100g2012apr_all, snp137NonFlagged, ljb2_sift and ljb_pp2.

WES was performed on the patient F2-IV-2 at the Baylor College of Medicine Human Genome Sequencing Center (BCM-HGSC) according to a previously described protocol (47). In brief, genomic DNA samples were prepared into Illumina paired-end libraries and underwent whole-exome capture via the BCM-HGSC core VCRome 2.1 design (48) (42 Mb, NimbleGen, Cat. No. 06266380001) according to the manufacturer's protocol (NimbleGen SeqCap EZ Exome Library SR User's Guide), followed by sequencing on the HiSeq 2000 platform (Illumina) with a sequencing yield of 8.4 Gb. The samples achieved 96% of the targeted exome bases covered to a depth-of-coverage of 20 or greater (49). Data produced were aligned and mapped to the human genome reference sequence (Genome Reference Consortium GRCh37, hg19) with the Mercury in-house bioinformatics pipeline (50). Variants were called using the ATLAS (an integrative variant analysis pipeline optimized for variant discovery) variant calling method and the Sequence Alignment/Map (SAMtools) suites and annotated with the in-house-developed 'Cassandra' annotation pipeline that uses Annotation of Genetic Variants ANNOVAR and additional tools and databases.

Variant prioritization for indels was as follows: If an indel is reported as a variant in the Human Gene Mutation Database (HGMD) and its frequency is less than 5% in the 1000 Genomes Project (1000GP) data, it was included. If it is not present in HGMD, it has to pass through all of the variant quality filters and its frequency has to be less than 2% in 1000GP data to be prioritized and investigated further as a potential pathogenic variant. In a second filtering step, another filter is further applied based on the number of samples having the variant in Atherosclerosis Risk in Communities Study (ARIC) database. The number of samples having the variant in the ARIC database should be less than 120 out of 10 940 samples in total.

Variant prioritization for single-nucleotide variants (SNVs) was as follows: If a SNV is reported as a variant in the HGMD or it has a clinical variant value between 3 and 8 in the Single Nucleotide Polymorphism database (dbSNP), its frequency has to be less than 5% in both 1000GP data and NHLBI GO Exome Sequencing Project (ESP5400) African and European populations. If it is not present in HGMD and does not have a clinical variant value between 3 and 8 in dbSNP, it has to pass through all of the variant quality filters and its frequency has to be less than 1% in both 1000GP data and ESP5400 African and European populations to be prioritized and investigated further as a potential pathogenic variant. Like indels, the SNVs that pass these filters were further filtered based on the number of samples having the variant in the ARIC database (should be less than 120 out of 10 940 samples in total). These filtering steps typically obtain ∼800 variants per sample (50).

Given the apparent autosomal recessive inheritance pattern in the pedigree we focused on the homozygous variants in the parsed and filtered WES data. Out of ∼800 variants, we selected the homozygous variants that have an allele frequency below 0.1% in our internal database (CMG), which consists of more than 6500 exomes including ∼ 1100 Turkish exomes. Then potential pathogenic variants including indels, nonsense and splice site variants, and missense variants that were predicted as deleterious in at least three out of five computational algorithms including SIFT, Polyphen2, LRT, Mutation Taster and PROVEAN, were selected as candidate variants. After these filtering steps five homozygous candidate variants in *BCL6*, *KDM1A*, *MRPS22*, *PLXND1* and *TRIM62* remained for manual inspection.

Sanger sequencing

The *MRPS22* (c.404G>A) variant was amplified by PCR using the following primers: 5′-ATG GCC TTA GTG GGA CAC AG-3′ and 5′-AGG AGC GAA ACT CCA TTT CA-3′. The 12 PCR amplicons that were not covered by WES in Family I on chromosome 3 between rs2737735 and rs16850488 were amplified and sequenced with the primers listed in Supplementary Material, Table S2. Sanger sequencing was performed by GenScript. The data were visualized and analyzed using FinchTV (Geospiza).

Genotyping

The *MRPS22* (c.404G>A) variant was amplified by PCR using the following primers: 5′-GAA AAT TAT TGG TGT CAA AAT TGT A-3′ and 5′-ATG GCC TTA GTG GGA CAC AG-3′. The resulting PCR product was digested with the Rsa1, and analyzed by agarose gel electrophoresis. Restriction digest of the wild-type PCR product resulted in a single 200 bp PCR product whereas restriction digest of the *MRPS22* (c.404G>A) variant resulted in a 176 bp and a 24 bp product.

Cell culture

For fibroblast cell lines, punch biopsies of skin were obtained from patients and controls. Patient and control fibroblast cell lines were cultured in high glucose Dulbecco's modified Eagle's medium (DMEM) (Thermo Fisher #11965-092) supplemented with 10% fetal bovine serum (Sigma, #F2442) and 1% penicillin and streptomycin (Thermo Fisher 15140-122).

Western blotting

Protein was extracted from cultured primary fibroblast cells with RIPA buffer (Sigma #R0278) and a protease inhibitor (Roche #05892791001). Protein was quantified using the BCA method. Western blotting was performed and quantitated using ImageJ as described (51). Primary antibodies used were an anti-MRPS22 monoclonal antibody (1: 1000, Proteintech #10984–1-AP) and an anti-alpha-tubulin antibody (1: 10 000, Sigma, #T9026). Secondary antibodies used were anti-rabbit (1: 5000, Thermo Fisher #31460) and anti-mouse (1: 5000, Thermo Fisher #31430).

Quantitative PCR (qPCR)

Total RNA was isolated from primary fibroblast cells using the PureLink RNA purification kit (Thermo Fisher) and reverse transcribed using the high capacity cDNA reverse transcription kit (Applied Biosystems). The sequences for qPCR primers are as follows: *MRPS22* forward primer 5′-TGA TAA TCA TGG CGC CCC TC-3′, *MRPS22* reverse primer 5′- CTA CCA GAT TCT GCG GCC T-3′; 12S rRNA forward primer 5′-TAG ATA CCC CAC TAT GCT TAG C-3′, 12S rRNA reverse primer 5′-CGA TTA CAG AAC AGG CTC C-3′; 16S rRNA forward primer 5′-CCA AAC CCA CTC CAC CTT AC-3′, 16S rRNA reverse primer 5′-TCA TCT TTC CCT TGC GGT AC-3′; *GAPDH* forward primer 5′-AAT CCC ATC ACC ATC TTC CA3′, *GAPDH* reverse primer 5'-TGG ACT CCA CGA CGT ACT CA3′. The qPCR reactions were performed with the power SYBR green PCR Master Mix (Thermo Fisher) and run on a Bio Rad CFX Connect Real Time System (Bio Rad). Expression levels were calculated using the △△Ct method relative to the *GAPDH* control gene.

Fibroblast oxidative phosphorylation and electron transport chain activity

Studies used an O2K (Oroboros Instruments) with permeabilized skin fibroblasts and performed with 2 protocols as described previously (52). Electron transport chain complexes in skin fibroblasts were measured spectrophotometrically at 37°C as described previously (53,54).

Mice

Heterozygous *Mrps22* knockout mice [B6N(Cg)-Mrps22tm1.1 (KOMP)Vlcg/J, stock #028462] were purchased from The Jackson Laboratory and maintained by brother-sister matings. All mice used for experiments were obtained from breeder colonies at Case Western Reserve University. Mice were housed in ventilated racks with access to food and water ad libitum and maintained at 21°C on a 12-h light/12-h dark cycle. All mice were cared for as described under the Guide for the Care and Use of Animals, eighth edition (2011) and all experiments were approved by IACUC and carried out in an AAALAC approved facility. The IACUC protocol number is 2014-0132. Mice were weaned at 3 weeks of age and genotyped. The *Mrps22* knockout allele was genotyped by PCR based on the presence of a 380 bp product (wild-type allele) or a 491 bp product (knockout allele). The sequence of the genotyping primers are as follows: *Mrps22* wild-type forward primer 5′-GCT GTG GGC AGT GTT ATT GT-3′, *Mrps22* wild-type reverse primer 5′-TCT CAC ACC TAG TAC CGC AGT C-3′; *Mrps22* mutant forward primer 5′-CGG TCG CTA CCA TTA CCA GT-3′, *Mrps22* mutant reverse primer 5′-TCA GTA AGT ACC TTT TAA TCC CAA GA-3′.

Drosophila stocks and culture conditions

All Drosophila strains used in this study were obtained from the Bloomington *Drosophila* Stock Center (BDSC), except for *c587-Gal4* which was a kind gift of T. Xie (Stowers Institute, Kansas City, MO). The stocks obtained from BDSC include *nos-Gal4* (BDSC #4937), *bab1-Gal4* (BDSC #6802), *tubP-Gal4* (BDSC #5138) and *mRpS22-P{TRiP.HMC06144}* (BDSC #65882). HMC RNAi lines are constructed in the VALIUM20 vector, designed for strong expression in both somatic and germline cells (55,56). To maximize knockdown expression, animals were raised at 29°C.

Immunofluorescence and image analysis

Drosophila ovaries from 2–3-day-old females were fixed and stained by standard methods (57). The primary Vasa antibody was obtained from the Developmental Studies Hybridoma Bank, and used at 1: 100. Secondary antibody conjugated to Alexa Fluor 555 (Thermo Fisher) was used at 1: 200. Images were acquired on a Leica TCS SP8 confocal microscope and assembled using Photoshop (Adobe) and PowerPoint (Microsoft).

Supplementary Material

Supplementary Material is available at *HMG* online.

Acknowledgements

The authors thank the Genome Aggregation Database (gnomAD) and the groups that provided exome and genome variant data to this resource. A full list of contributing groups

can be found on their website. We also thank the Research Institute for Children's Health at Case Western Reserve University and its director, Dr Mitchell Drumm, for support and guidance. This work made use of the High Performance Computing Resource in the Core Facility for Advanced Research Computing at Case Western Reserve University.

Conflict of Interest statement. J.R.L. has stock ownership in 23andMe and Lasergen, is a paid consultant for Regeneron Pharmaceuticals, and is a coinventor on multiple United States and European patents related to molecular diagnostics for inherited neuropathies, eye diseases and bacterial genomic fingerprinting. The Department of Molecular and Human Genetics at Baylor College of Medicine derives revenue from the chromosomal microarray analysis and clinical exome sequencing offered in the Baylor Genetics Laboratory.

Funding

This work was supported by the National Institute of Diabetes and Digestive and Kidney Diseases (NIDDK) [grant numbers DK099533 and DK112846 to D.A.B.], the Sigma Xi Scientific Research Society [grant number G201603152079889 to A.C.], the National Institute of General Medical Sciences (NIGMS) [grant number GM102141 to H.K.S.], and the US National Human Genome Research Institute/National Heart Lung and Blood Institute (NHGRI/NHLBI) supported Baylor Hopkins Center for Mendelian Genetics (BHCMG) [grant number UM1 HG006542]. We would also like to acknowledge use of the Leica SP8 confocal microscope in the Light Microscopy Imaging Facility at Case Western Reserve University made available through the National Institutes of Health - Office of Research Infrastructure Programs (NIH-ORIP) shared instrumentation grant [grant number S10OD016164]. Stocks obtained from the Bloomington Drosophila Stock Center were used in this study which is supported by the Office of the Director of the National Institutes of Health (NIH) [grant number P40OD018537] .

References

1. Committee opinion no. 605: primary ovarian insufficiency in adolescents and young women (2014) *Obstet. Gynecol.*, **124**, 193–197.
2. Rossetti, R., Ferrari, I., Bonomi, M. and Persani, L. (2017) Genetics of primary ovarian insufficiency: genetics of POI. *Clin. Genet.*, **91**, 183–198.
3. Bolcun-Filas, E., Hall, E., Speed, R., Taggart, M., Grey, C., de Massy, B., Benavente, R. and Cooke, H.J. (2009) Mutation of the mouse *Syce1* gene disrupts synapsis and suggests a link between synaptonemal complex structural components and DNA repair. *PLoS Genet.*, **5**, e1000393.
4. Costa, Y., Speed, R., Ollinger, R., Alsheimer, M., Semple, C.A., Gautier, P., Maratou, K., Novak, I., Höög, C., Benavente, R. *et al.* (2005) Two novel proteins recruited by synaptonemal complex protein 1 (SYCP1) are at the centre of meiosis. *J. Cell Sci.*, **118**, 2755–2762.
5. Caburet, S., Arboleda, V.A., Llano, E., Overbeek, P.A., Barbero, J.L., Oka, K., Harrison, W., Vaiman, D., Ben-Neriah, Z., García-Tuñón, I. *et al.* (2014) Mutant cohesin in premature ovarian failure. *N. Engl. J. Med.*, **370**, 943–949.
6. Guiraldelli, M.F., Eyster, C., Wilkerson, J.L., Dresser, M.E. and Pezza, R.J. (2013) Mouse HFM1/Mer3 is required for crossover formation and complete synapsis of homologous chromosomes during meiosis. *PLoS Genet.*, **9**, e1003383.
7. Wang, J., Zhang, W., Jiang, H. and Wu, B.-L. and Primary Ovarian Insufficiency Collaboration (2014) Mutations in *HFM1* in recessive primary ovarian insufficiency. *N. Engl. J. Med.*, **370**, 972–974.
8. Weinberg-Shukron, A., Renbaum, P., Kalifa, R., Zeligson, S., Ben-Neriah, Z., Dreifuss, A., Abu-Rayyan, A., Maatuk, N., Fardian, N., Rekler, D. *et al.* (2015) A mutation in the nucleoporin-107 gene causes XX gonadal dysgenesis. *J. Clin. Invest.*, **125**, 4295–4304.
9. AlAsiri, S., Basit, S., Wood-Trageser, M.A., Yatsenko, S.A., Jeffries, E.P., Surti, U., Ketterer, D.M., Afzal, S., Ramzan, K., Faiyaz-Ul Haque, M. *et al.* (2015) Exome sequencing reveals *MCM8* mutation underlies ovarian failure and chromosomal instability. *J. Clin. Invest.*, **125**, 258–262.
10. Fauchereau, F., Shalev, S., Chervinsky, E., Beck-Fruchter, R., Legois, B., Fellous, M., Caburet, S. and Veitia, R.A. (2016) A non-sense *MCM9* mutation in a familial case of primary ovarian insufficiency. *Clin. Genet.*, **89**, 603–607.
11. Wood-Trageser, M.A., Gurbuz, F., Yatsenko, S.A., Jeffries, E.P., Kotan, L.D., Surti, U., Ketterer, D.M., Matic, J., Chipkin, J., Jiang, H. *et al.* (2014) *MCM9* mutations are associated with ovarian failure, short stature, and chromosomal instability. *Am. J. Hum. Genet.*, **95**, 754–762.
12. Zhao, H., Chen, Z.-J., Qin, Y., Shi, Y., Wang, S., Choi, Y., Simpson, J.L. and Rajkovic, A. (2008) Transcription factor *FIGLA* is mutated in patients with premature ovarian failure. *Am. J. Hum. Genet.*, **82**, 1342–1348.
13. Bayram, Y., Gulsuner, S., Guran, T., Abaci, A., Yesil, G., Gulsuner, H.U., Atay, Z., Pierce, S.B., Gambin, T., Lee, M. *et al.* (2015) Homozygous loss-of-function mutations in *SOHLH1* in patients with nonsyndromic hypergonadotropic hypogonadism. *J. Clin. Endocrinol. Metab.*, **100**, E808–E814.
14. Qin, Y., Choi, Y., Zhao, H., Simpson, J.L., Chen, Z.-J. and Rajkovic, A. (2007) *NOBOX* homeobox mutation causes premature ovarian failure. *Am. J. Hum. Genet.*, **81**, 576–581.
15. Bouilly, J., Bachelot, A., Broutin, I., Touraine, P. and Binart, N. (2011) Novel *NOBOX* loss-of-function mutations account for 6.2% of cases in a large primary ovarian insufficiency cohort. *Hum. Mutat.*, **32**, 1108–1113.
16. Kasippillai, T., MacArthur, D.G., Kirby, A., Thomas, B., Lambalk, C.B., Daly, M.J. and Welt, C.K. (2013) Mutations in *eIF4ENIF1* are associated with primary ovarian insufficiency. *J. Clin. Endocrinol. Metab.*, **98**, E1534–E1539.
17. Kurolap, A., Orenstein, N., Kedar, I., Weisz Hubshman, M., Tiosano, D., Mory, A., Levi, Z., Marom, D., Cohen, L., Ekhilevich, N. *et al.* (2016) Is one diagnosis the whole story? Patients with double diagnoses. *Am. J. Med. Genet. A*, **170**, 2338–2348.
18. Rösler, A., Silverstein, S. and Abeliovich, D. (1996) A (R80Q) mutation in 17 beta-hydroxysteroid dehydrogenase type 3 gene among Arabs of Israel is associated with pseudohermaphroditism in males and normal asymptomatic females. *J. Clin. Endocrinol. Metab.*, **81**, 1827–1831.
19. Geissler, W.M., Davis, D.L., Wu, L., Bradshaw, K.D., Patel, S., Mendonca, B.B., Elliston, K.O., Wilson, J.D., Russell, D.W. and Andersson, S. (1994) Male pseudohermaphroditism caused by mutations of testicular 17β–hydroxysteroid dehydrogenase 3. *Nat. Genet.*, **7**, 34–39.
20. Mendonca, B.B., Arnhold, I.J.P., Bloise, W., Andersson, S., Russell, D.W. and Wilson, J.D. (1999) 17β-Hydroxysteroid Dehydrogenase 3 Deficiency In Women. *J. Clin. Endocrinol. Metab.*, **84**, 802–804.
21. Ng, P.C. and Henikoff, S. (2003) SIFT: predicting amino acid changes that affect protein function. *Nucleic Acids Res.*, **31**, 3812–3814.

22. Adzhubei, I., Jordan, D.M. and Sunyaev, S.R. (2013) Predicting functional effect of human missense mutations using PolyPhen-2. *Curr. Protoc. Hum. Genet.*, Chapter 7, Unit7.20.
23. Sobreira, N., Schiettecatte, F., Valle, D. and Hamosh, A. (2015) GeneMatcher: a matching tool for connecting investigators with an interest in the same gene. *Hum. Mutat.*, **36**, 928–930.
24. Scott, E.M., Halees, A., Itan, Y., Spencer, E.G., He, Y., Azab, M.A., Gabriel, S.B., Belkadi, A., Boisson, B., Abel, L. *et al.* (2016) Characterization of Greater Middle Eastern genetic variation for enhanced disease gene discovery. *Nat. Genet.*, **48**, 1071–1076.
25. Lek, M., Karczewski, K.J., Minikel, E.V., Samocha, K.E., Banks, E., Fennell, T., O'Donnell-Luria, A.H., Ware, J.S., Hill, A.J., Cummings, B.B. *et al.* (2016) Analysis of protein-coding genetic variation in 60, 706 humans. *Nature*, **536**, 285–291.
26. Saada, A., Shaag, A., Arnon, S., Dolfin, T., Miller, C., Fuchs-Telem, D., Lombes, A. and Elpeleg, O. (2007) Antenatal mitochondrial disease caused by mitochondrial ribosomal protein (*MRPS22*) mutation. *J. Med. Genet.*, **44**, 784–786.
27. Smits, P., Saada, A., Wortmann, S.B., Heister, A.J., Brink, M., Pfundt, R., Miller, C., Haas, D., Hantschmann, R., Rodenburg, R.J.T. *et al.* (2011) Mutation in mitochondrial ribosomal protein *MRPS22* leads to Cornelia de Lange-like phenotype, brain abnormalities and hypertrophic cardiomyopathy. *Eur. J. Hum. Genet.*, **19**, 394–399.
28. Lee, T. and Luo, L. (1999) Mosaic analysis with a repressible cell marker for studies of gene function in neuronal morphogenesis. *Neuron*, **22**, 451–461.
29. Cabrera, G.R., Godt, D., Fang, P.-Y., Couderc, J.-L. and Laski, F.A. (2002) Expression pattern of Gal4 enhancer trap insertions into the *bric à brac* locus generated by P element replacement. *Genesis*, **34**, 62–65.
30. Van Doren, M., Williamson, A.L. and Lehmann, R. (1998) Regulation of zygotic gene expression in Drosophila primordial germ cells. *Curr. Biol.*, **8**, 243–246.
31. Smits, P., Smeitink, J.A.M., van den Heuvel, L.P., Huynen, M.A. and Ettema, T.J.G. (2007) Reconstructing the evolution of the mitochondrial ribosomal proteome. *Nucleic Acids Res.*, **35**, 4686–4703.
32. Greber, B.J. and Ban, N. (2016) Structure and Function of the Mitochondrial Ribosome. *Annu. Rev. Biochem.*, **85**, 103–132.
33. Amunts, A., Brown, A., Toots, J., Scheres, S.H.W. and Ramakrishnan, V. (2015) Ribosome. The structure of the human mitochondrial ribosome. *Science*, **348**, 95–98.
34. Greber, B.J., Bieri, P., Leibundgut, M., Leitner, A., Aebersold, R., Boehringer, D. and Ban, N. (2015) Ribosome. The complete structure of the 55S mammalian mitochondrial ribosome. *Science*, **348**, 303–308.
35. Menezes, M.J., Guo, Y., Zhang, J., Riley, L.G., Cooper, S.T., Thorburn, D.R., Li, J., Dong, D., Li, Z., Glessner, J. *et al.* (2015) Mutation in mitochondrial ribosomal protein S7 (*MRPS7*) causes congenital sensorineural deafness, progressive hepatic and renal failure and lactic acidemia. *Hum. Mol. Genet.*, **24**, 2297–2307.
36. Pierce, S.B., Chisholm, K.M., Lynch, E.D., Lee, M.K., Walsh, T., Opitz, J.M., Li, W., Klevit, R.E. and King, M.-C. (2011) Mutations in mitochondrial histidyl tRNA synthetase *HARS2* cause ovarian dysgenesis and sensorineural hearing loss of Perrault syndrome. *Proc. Natl. Acad. Sci. U. S. A.*, **108**, 6543–6548.
37. Pierce, S.B., Gersak, K., Michaelson-Cohen, R., Walsh, T., Lee, M.K., Malach, D., Klevit, R.E., King, M.-C. and Levy-Lahad, E. (2013) Mutations in *LARS2*, encoding mitochondrial leucyl-tRNA synthetase, lead to premature ovarian failure and hearing loss in Perrault syndrome. *Am. J. Hum. Genet.*, **92**, 614–620.
38. Dallabona, C., Diodato, D., Kevelam, S.H., Haack, T.B., Wong, L.-J., Salomons, G.S., Baruffini, E., Melchionda, L., Mariotti, C., Strom, T.M. *et al.* (2014) Novel (ovario) leukodystrophy related to *AARS2* mutations. *Neurology*, **82**, 2063–2071.
39. Fogli, A., Rodriguez, D., Eymard-Pierre, E., Bouhour, F., Labauge, P., Meaney, B.F., Zeesman, S., Kaneski, C.R., Schiffmann, R. and Boespflug-Tanguy, O. (2003) Ovarian failure related to eukaryotic initiation factor 2B mutations. *Am. J. Hum. Genet.*, **72**, 1544–1550.
40. Baertling, F., Haack, T.B., Rodenburg, R.J., Schaper, J., Seibt, A., Strom, T.M., Meitinger, T., Mayatepek, E., Hadzik, B., Selcan, G. *et al.* (2015) *MRPS22* mutation causes fatal neonatal lactic acidosis with brain and heart abnormalities. *Neurogenetics*, **16**, 237–240.
41. Kılıç, M., Oğuz, K.-K., Kılıç, E., Yüksel, D., Demirci, H., Sağıroğlu, M.Ş., Yücel-Yılmaz, D. and Özgül, R.K. (2017) A patient with mitochondrial disorder due to a novel mutation in *MRPS22*. *Metab. Brain Dis.*, 10.1007/s11011-017-0074-5.
42. May-Panloup, P., Boucret, L., Chao de la Barca, J.-M., Desquiret-Dumas, V., Ferré-L'Hotellier, V., Morinière, C., Descamps, P., Procaccio, V. and Reynier, P. (2016) Ovarian ageing: the role of mitochondria in oocytes and follicles. *Hum. Reprod. Update*, **22**, 725–743.
43. Hayashi, Y., Otsuka, K., Ebina, M., Igarashi, K., Takehara, A., Matsumoto, M., Kanai, A., Igarashi, K., Soga, T. and Matsui, Y. (2017) Distinct requirements for energy metabolism in mouse primordial germ cells and their reprogramming to embryonic germ cells. *Proc. Natl. Acad. Sci. U. S. A.*, **114**, 8289–8294.
44. Li, H. and Durbin, R. (2009) Fast and accurate short read alignment with Burrows-Wheeler transform. *Bioinforma. Oxf. Engl.*, **25**, 1754–1760.
45. McKenna, A., Hanna, M., Banks, E., Sivachenko, A., Cibulskis, K., Kernytsky, A., Garimella, K., Altshuler, D., Gabriel, S., Daly, M. *et al.* (2010) The Genome Analysis Toolkit: a MapReduce framework for analyzing next-generation DNA sequencing data. *Genome. Res.*, **20**, 1297–1303.
46. Wang, K., Li, M. and Hakonarson, H. (2010) ANNOVAR: functional annotation of genetic variants from high-throughput sequencing data. *Nucleic Acids Res.*, **38**, e164.
47. Lupski, J.R., Gonzaga-Jauregui, C., Yang, Y., Bainbridge, M.N., Jhangiani, S., Buhay, C.J., Kovar, C.L., Wang, M., Hawes, A.C., Reid, J.G. *et al.* (2013) Exome sequencing resolves apparent incidental findings and reveals further complexity of *SH3TC2* variant alleles causing Charcot-Marie-Tooth neuropathy. *Genome Med.*, **5**, 57.
48. Bainbridge, M.N., Wang, M., Wu, Y., Newsham, I., Muzny, D.M., Jefferies, J.L., Albert, T.J., Burgess, D.L. and Gibbs, R.A. (2011) Targeted enrichment beyond the consensus coding DNA sequence exome reveals exons with higher variant densities. *Genome Biol.*, **12**, R68.
49. Challis, D., Yu, J., Evani, U.S., Jackson, A.R., Paithankar, S., Coarfa, C., Milosavljevic, A., Gibbs, R.A. and Yu, F. (2012) An integrative variant analysis suite for whole exome next-generation sequencing data. *BMC Bioinformatics*, **13**, 8.
50. Reid, J.G., Carroll, A., Veeraraghavan, N., Dahdouli, M., Sundquist, A., English, A., Bainbridge, M., White, S., Salerno, W., Buhay, C. *et al.* (2014) Launching genomics into the cloud: deployment of Mercury, a next generation sequence analysis pipeline. *BMC Bioinformatics*, **15**, 30.
51. Charrier, A., Wang, L., Stephenson, E.J., Ghanta, S.V., Ko, C.-W., Croniger, C.M., Bridges, D. and Buchner, D.A. (2016) Zinc

finger protein 407 overexpression upregulates PPAR target gene expression and improves glucose homeostasis in mice. *Am. J. Physiol. Endocrinol. Metab.*, **311**, E869–E880.
52. Ye, F. and Hoppel, C.L. (2013) Measuring oxidative phosphorylation in human skin fibroblasts. *Anal. Biochem.*, **437**, 52–58.
53. Hoppel, C.L., Kerr, D.S., Dahms, B. and Roessmann, U. (1987) Deficiency of the reduced nicotinamide adenine dinucleotide dehydrogenase component of complex I of mitochondrial electron transport. Fatal infantile lactic acidosis and hypermetabolism with skeletal-cardiac myopathy and encephalopathy. *J. Clin. Invest.*, **80**, 71–77.
54. Krähenbühl, S., Talos, C., Wiesmann, U. and Hoppel, C.L. (1994) Development and evaluation of a spectrophotometric assay for complex III in isolated mitochondria, tissues and fibroblasts from rats and humans. *Clin. Chim. Acta Int. J. Clin. Chem.*, **230**, 177–187.
55. Ni, J.-Q., Zhou, R., Czech, B., Liu, L.-P., Holderbaum, L., Yang-Zhou, D., Shim, H.-S., Tao, R., Handler, D., Karpowicz, P. *et al.* (2011) A genome-scale shRNA resource for transgenic RNAi in Drosophila. *Nat. Methods*, **8**, 405–407.
56. Perkins, L.A., Holderbaum, L., Tao, R., Hu, Y., Sopko, R., McCall, K., Yang-Zhou, D., Flockhart, I., Binari, R., Shim, H.-S. *et al.* (2015) The transgenic RNAi project at Harvard Medical School: resources and validation. *Genetics*, **201**, 843–852.
57. Shapiro-Kulnane, L., Smolko, A.E. and Salz, H.K. (2015) Maintenance of Drosophila germline stem cell sexual identity in oogenesis and tumorigenesis. *Dev. Camb. Engl.*, **142**, 1073–1082.